Romanian Reports in Physics, Vol. 66, No. 3, P. 788–800, 2014

ULTRA HIGH MOLECULAR WEIGHT POLYETHYLENE ACETABULAR CUPS FUNCTIONALIZED WITH BIOACTIVE GLASS COATINGS SYNTHESIZED BY PULSED LASER DEPOSITION

L. DUTA[1], A. C. POPA[2,3,4], F. MICULESCU[5], I. N. MIHAILESCU[1,*]

[1] National Institute for Lasers, Plasma and Radiation Physics, Lasers Department, Magurele-Ilfov, Romania, E-mail: liviu.duta@inflpr.ro, E-mail*: ion.mihailescu@inflpr.ro
[2] Army Centre for Medical Research, Bucharest, Romania, E-mail: adrian_popa_mailbox@yahoo.com
[3] "Carol Davila" University of Medicine and Pharmacy, Department of Cellular and Molecular Medicine, Bucharest, Romania
[4] National Institute of Materials Physics, Magurele-Ilfov, Romania
[5] "Politehnica" University of Bucharest, Faculty of Materials Science and Engineering, Bucharest, Romania, E-mail: f_miculescu@yahoo.com

Received September 26, 2013

Abstract. We report on the synthesis by PLD of bioactive glass (BG) films onto ultra high molecular weight polyethylene acetabular cups, and their preliminarily characterization after immersion in simulated body fluid. Fourier Transform Infrared spectra evidenced the strong depolymerization of the BG coatings. Scanning Electron Microscopy evidenced that the typical PLD film surface was converted after soaking in SBF to a rough one consisting of acicular crystals. Energy Dispersive Spectroscopy analysis demonstrated a remarkable conservation of the targets stoichiometry. The functionalization of acetabular cups with BG films by PLD should allow for the fabrication of implant coatings with improved osteoinductive characteristics.

Key words: bioactive glass, UHMWPE acetabular cup, pulsed laser deposition, SBF immersion, regenerative medicine.

1. INTRODUCTION

The total joint replacement (TJR) is a common treatment in degenerative joint diseases. A conventional TJR consists of metallic implant convex component (fabricated from cobalt-chromium or titanium medical grade alloys) articulating against an ultra-high molecular weight polyethylene (UHMWPE) concave component [1]. Prosthesis loosening because of an improper in situ anchoring is one of the main post-operative complications and new solutions are under study.

Two methods of fixation are commonly used, namely: (*i*) cementation, and (*ii*) functionalization with osteointegrative coatings able to stimulate rapid bone in-growth (e.g. hydroxyapatite [HA, $Ca_{10}(PO_4)_6(OH)_2$] [1, 2–5]). The second one is mostly applied in case of younger patients due to a superior quality of bone and rapid self-healing process. The main task of orthopedic devices is to stimulate bone regeneration, and therefore, they should be bioactive. Calcium phosphates (CaPs) have been intensively studied for their chemical and structural similarity to the mineral part of bone [2]. Because bulk ceramics are very brittle and cannot withstand high mechanical loads, devices fabricated completely out of these materials are unsuitable. A solution is to use metals or polymers as main implant support, covered by a thin and adherent ceramic or glass layer, making the surface bioactive, and thus stimulating the osteogenic cell differentiation and bone matrix growth [2–4, 6, 7].

UHMWPE is a polymer with excellent properties: very low coefficient of friction, self-lubricating, inert, low weight, high corrosion resistance, excellent aesthetics, and ease of manufacture. It is also a very tough material, possessing one of the highest impact strength of the thermoplastics known [8]. UHMWPE has more than 50 years of clinical history and emerged as the dominant bearing biomaterial for use in artificial joint (e.g. hip, knee) replacements and for spine implants [9]. Despite its success in restorative medicine, such orthopedic and spine implants do not exhibit osteointegration abilities, and so, have limited lifetime, requiring periodic revision surgeries.

Bioactive glasses (BG) are recognized to be osteoproductive materials [10, 11]. They are composed of various metal oxide compositions. Their composition is changing *in vivo* in contact with body fluids, partially converting to a biological apatite [11]. Since the pioneering works of Hench *et al*., in early ’70 [12], BGs have attracted an increased attention towards clinical applications due to their superior bioactivity (as compared to CaPs), osteoinductivity and biodegradability characteristics [13–15]. Hench [13] demonstrated that, when BG materials are immersed in a physiological environment, a sequence of five stages is initiated resulting in the formation of a carbonated apatite (CHA) layer: (*i*) migration of Na, K, Ca ions in the extracellular fluids; (*ii*) hydrolysis, in which Si–O–Si covalent bonds are shattered, resulting in Si–OH groups formation, and the glass network is disrupted; (*iii*) total condensation of Si–OH groups, by which the disrupted glass network changes its morphology to form a gel-like surface layer, depleted of Ca and alkaline ions; (*iv*) precipitation of an amorphous CaP on top of the SiO_2 gel layer; (*v*) mineralization of the CaP layer followed by gradual transformation to a biologically active CHA, that mimics the mineral phase naturally contained in bones [16].

Various techniques, such as plasma spraying [17, 18], sol-gel [19], electrophoretic deposition [20, 21], enameling [17], radio-frequency magnetron sputtering [22, 23] and pulsed laser deposition (PLD) [24–26] have been proposed to prepare high quality BG coatings.

In PLD technique, the substance is expulsed from target under the action of multipulse laser irradiation and transferred to a nearby substrate. PLD presents numerous advantages in respect to the aforementioned deposition techniques, such as: accurate control of the deposited material's stoichiometry, reduced film contamination due to the use of laser light, energy source placed outside the deposition environment, relative simplicity of the growth facility offering great experimental versatility (multilayers, doping), and a precise thickness control (10^{-2} nm/pulse). PLD can be applied to the synthesis of both well-separated nanoparticle assemblies [27, 28] or continuous adherent bioactive films [24, 29, 30].

The goal of this study is to assess the feasibility of the biofunctionalizion of UHMWPE acetabular cup implants by PLD. To the best of our knowledge, this is the first study in literature reporting on the 3D UHMWPE acetabular cups functionalization with BG thin films for orthopedic applications.

2. EXPERIMENTAL

2.1. BIOGLASS COMPOSITION

We used a BG powder from the SiO_2–Na_2O–K_2O–CaO–MgO–P_2O_5 compositional system, containing 61 wt.% SiO_2 (further denoted as BG61), reckoned for its excellent biological potential [24, 31, 32]. The weight BG61 powder composition is given in Table 1.

Table 1

Composition (in wt. %) of BG61 powder used for depositions

Powder	**Oxide [wt. %]**					
	SiO_2	Na_2O	K_2O	CaO	MgO	P_2O_5
BG61	61.1	10.3	2.8	12.6	7.2	6

2.2. PLD EXPERIMENT

PLD deposition was conducted inside a stainless steel reaction chamber using a KrF* excimer laser source (λ = 248 nm, $\tau_{FWHM} \leq 25$ ns), running at a repetition rate of 10 Hz. The laser beam was incident onto the target surface at 45°. Three grams of BG61 powder were pressed at 4 t in a 2 cm diameter mold and the resulting pellets were heat-treated in a furnace at 650°C for six hours to reach compactness by eliminating air bubbles and water vapors. The resulted compact pellets were used as targets in PLD experiments. The ablated material was collected onto commercial UHMWPE cotyle implants, having diameters in the range of 28–36 mm. They were placed parallel to the targets (on-axis geometry), at

4 cm separation distance. Prior to introduction inside the deposition chamber, the substrates were successively cleaned using a laboratory protocol described elsewhere [30, 33], in order to eliminate contaminants. The incident laser fluence on target was set at ~3 J/cm^2. Because of the polymeric nature of the substrate, prone to thermal degradation if the temperature of the deposition process is in excess of the softening point at ~80°C, all experiments were conducted at room temperature (RT). For the growth of one thin film, 15000 consecutive laser pulses were applied. In order to avoid drilling as the effect of multipulse laser irradiation, the targets were continuously rotated at 0.4 Hz and translated along two orthogonal axes. This procedure also allowed for the deposition of an uniform film. All depositions were carried out in a flux of 1.5x10^{-3} Pa O_2. We mention that the use of an O_2 ambient is essential for the reconstitution of the complex stoichiometry of the deposited compound.

2.3. CHARACTERIZATION OF DEPOSITED STRUCTURES

Fourier transform infrared (FTIR) spectroscopy studies were performed using a Perkin Elmer BX Spectrum-Pike spectrometer in Attenuated Total Reflectance mode for the detection of the functional groups present in the BG61 films before and after immersion in simulated body fluid (SBF). The analysis was carried out within the (4000 – 550) cm^{-1} range, with a 4 cm^{-1} resolution, and a total of 100 scans/experiment.

The surface morphology of the BG61 coatings was monitored by low vacuum (~106 Pa) scanning electron microscopy (SEM), using a Philips XL30 installation. No conductive coating was applied.

The elemental composition analysis was conducted by energy dispersive spectroscopy (EDS), using a Sapphire-UTW EDAX instrument, at an acceleration voltage of 20 keV, and mediating over a surface area of (50x50) μm^2.

The biomineralization capacity of the UHMWPE acetabular cups biofunctionalized with PLD glass coatings was investigated by immersion in SBF, complying with the standard ISO bioactivity testing protocol [34]. The SBF solution had the following ionic concentrations (in mMol): 142.0 Na^+, 5.0 K^+, 2.5 Ca^{2+}, 1.5 Mg^{2+}, 147.8 Cl^-, 4.2 HCO^{3-}, 1.0 HPO_4^{2-} and 0.5 SO_4^{2-}. The solutions are buffered at pH = 7.4 with tris-hydroxymethyl-amminomethane (Tris, 50 mM) and hydrochloric acid solutions according to the recipe introduced by T. Kokubo [35]. The SBF was filtered through sterilized Millipore PVDF type filters with 0.22 μm pore size. Sterilized polystyrene bottles were used for tests. A surface area to volume ratio of 0.1 cm^{-1} was maintained for all immersions [34], while the SBF solution was periodically refreshed during experiments. Sampling was performed after 42 days of immersion in SBF. After soaking, the samples were extracted from SBF, rinsed gently, first with ethanol and then with deionised water and let to dry at RT in a desiccator.

3. RESULTS AND DISCUSSION

3.1. FTIR

Figure 1 shows the FTIR spectra of BG61 films, before and after 42 days of immersion in SBF. For comparison, we also provided the FTIR spectra of bare UHMWPE substrate (black solid line in Fig. 1) and of a pure HA powder (Sigma Aldrich) (green dotted line in Fig. 2b).

The five sharp IR bands at 2916, 2848, 1464, 731 and 718 cm^{-1}, are characteristic to UHMWPE, and correspond to following vibration modes: asymmetric stretching of the $–CH_2$ aliphatic groups, symmetric stretching of the $–CH_2$ aliphatic groups, C–H bending deformation, $=CH_2$ out-of-plane bending and C–H rocking deformation, respectively (Table 2) [36].

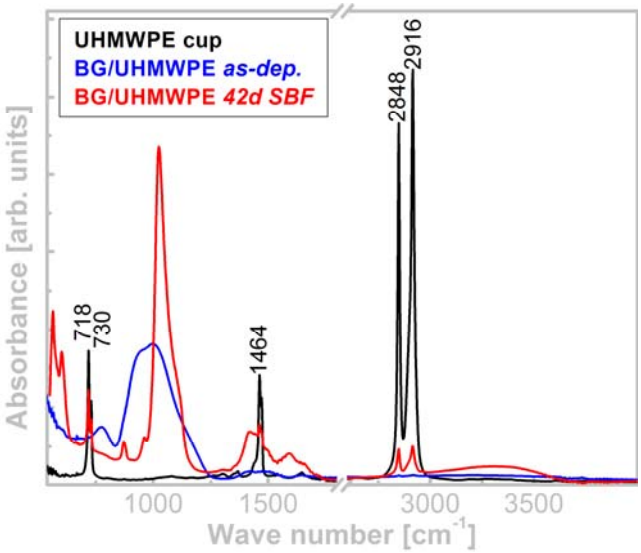

Fig. 1 – FTIR spectra of UHMWPE substrate (black line) and BG61 coatings prior (blue line) and after (red line) 42 days of immersion in SBF.

In Fig. 2 one can observe the detailed FTIR spectra of BG61 samples for two different wave number domains: (1750–550) and (4000–2500) cm^{-1}, respectively. The lower intensity spectrum (blue line) belongs to the as-deposited BG61 coating, whilst the one with sharper peaks (red line) was recorded in case of the implant coating after 42 days of immersion in SBF.

The peaks at 776, 942, 1002 and 1140 cm^{-1} (Fig. 2a), visible before immersion in SBF, belong to vibration modes specific to Si–O– bonds (Table 2) in various tetrahedral units [22, 37–39]. A depolymerized silica network, such as the one of a BG containing high concentration of alkali and alkali earth elements,

possesses two types of oxygen atoms. They are: bridging oxygens (BOs), which cross-link the entire tri-dimensional silicate network, and non-bridging oxygens (NBOs), generated by the network modifiers (e.g. K^+, Na^+, Ca^{2+}, Mg^{2+} cations), whose charge is compensated by breaking the BOs bonds. We note that structural Q^n silicate species with low n values (were n stands for the number of BOs) are common in BG materials. It is to mention that a relative high concentration of NBOs is favorable to an increased bioactivity [22, 40]. Due to the low content of P in the selected BG composition, the absorbance bands of phosphate units (typically orthophosphate groups [41]), occurring in the (1400 – 400) cm^{-1} IR spectra range [37], are superimposed to the more intense silicate group bands.

After 42 days of immersion in SBF (Fig. 2a, red line), remarkable structural changes are noticed. The BG61 film bands, previously dominant, are now obscured by new and stronger bands emerging at 564, 602, 872, 962, 1025, 1102, 1423, 1495 and 1592 cm^{-1}. The prominent IR band with three peaking shoulders belong to the vibration bands of phosphate functional groups in HA: ν_1 symmetric stretching mode (962 cm^{-1}) and degenerated asymmetric stretching modes (1024 and 1102 cm^{-1}) [38, 42, 43]. The sharpness and splitting of the ν_4 symmetric stretching of phosphate (placed at 564 and 602 cm^{-1}, respectively) are indicative of a well-crystallized HA [42]. The structure of the HA layer growing *in vitro* is strongly hydroxylated and carbonated. This was revealed by the presence of important hydroxyl and carbonate vibrational bands: H–O–H (ν_2) bending mode (1592 cm^{-1}), $(OH)^-$ groups of absorbed water (broad band in the range 3700 – 2700 cm^{-1}), $(CO_3)^{2-}$ (ν_2) bending mode (872 cm^{-1}) and the $(CO_3)^{2-}$ (ν_3) degenerated asymmetric stretching modes (1423 and 1495 cm^{-1}). The positions of the carbonate IR bands advocate for a B-type carbonate substitution (replacing the phosphate ions [42]), typical also for human bone [44]. The absence of the OH structural librational mode (~630 cm^{-1}), as well as the slight shift of the phosphate bands (inset to Fig. 2a) to higher wavelengths with respect to the IR bands present in the pure HA spectrum, plead for the non-stoichiometric apatitic nature of the layer developed and biomineralized in SBF [39]. We note that the mineral part of bone is in fact a non-stoichiometric B-type carbonated HA, with reduced crystallinity, and substantial level of doping (e.g. $(CO_2)^{-3}$ (3–8 wt.%), ~0.5 wt.% Mg^{2+}, or ~0.7 wt.% Na^+) [44, 45].

The transformation in SBF is in agreement to the Hench bioactivity mechanism [13]. The HA nucleation on top of BG61-functionalized implants is the effect of partial dissolution of the glass matrix. These phenomena were found to be linked to the formation of silicic acid and successive polycondensation reactions, along with the beginning of the precipitation on the surface of CaPs phases from the SBF solution, which is supersaturated in Ca and P ions [13]. The released water in the polycondensation reaction remains physically bonded with the Si–O–Si surface forming the hydrated silica rich layer [10]. This leads to a pH increase at the surface level which favors the absorption of the cations and anions on the surface. Under these favorable conditions, the precipitation processes of CaP rich phases are enhanced.

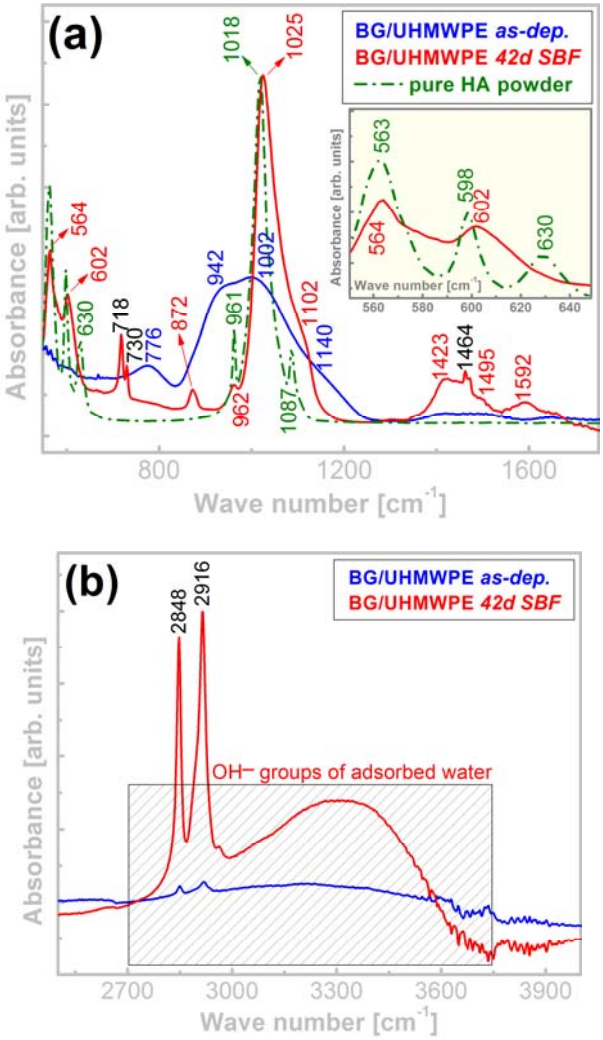

Fig. 2 – Detailed FTIR spectra of BG61 coatings prior (blue line) and after (red line) the immersion in SBF for 42 days: a) 1750–550; b) 4000–2500 cm^{-1} range zoom.

Table 2

Assignment of the IR bands evidenced before and after 42 days of immersion in SBF of BG61 samples

FTIR BANDS [cm^{-1}]		**ASSIGNMENT**
BG61 film as-deposited	**BG film immersed in SBF**	
–	564	$(PO_4)^{3-}$ (ν_4) bending mode [37,38,39,42,43]
–	602	$(PO_4)^{3-}$ (ν_4) bending mode [37,38,39,42,43]
–	718	C–H rocking deformation [36]
–	730	$=CH_2$ out-of-plane bending [36]

Table 2 (continued)

776	–	Si–O bending vibration mode [23,37,38,39]
–	872	$(CO_3)^{2-}$ (ν_2) bending mode [37,38,39,42,43]
942	–	Si–O vibrations in Q^2 units [23,37,38,39]
–	962	$(PO_4)^{3-}$ (ν_1) symmetric stretching mode [37,38,39,42,43]
1002	–	Si–O vibrations in Q^3 units [23,37,38,39]
–	1025	$(PO_4)^{3-}$ (ν_3) asymmetric stretching mode [37,38,39,42,43]
–	1102	$(PO_4)^{3-}$ (ν_3) symmetric stretching mode [37,38,39,42,43]
1140	–	Si–O vibrations in Q^4 units [23,37,38,39]
–	1423	$(CO_3)^{2-}$ (ν_3) asymmetric stretching mode [37,38,39,42,43]
–	1464	C–H bending deformation [36]
–	1495	$(CO_3)^{2-}$ (ν_3) asymmetric stretching mode [37,38,39,42,43]
–	1592	H–O–H (ν_2) bending mode [37,38,39,42]
2848	2848	symmetric stretching of aliphatic $-CH_2$ groups [36]
2916	2916	asymmetric stretching of aliphatic $-CH_2$ groups [36]
–	3700 – 2700	$(OH)^-$ groups of absorbed water [37,38,39,42]

3.2. MACROSCOPIC AND MICROSCOPIC STUDIES

We present in Fig. 3 the photos acquired in case of a bare and functionalized (with BG61 thin film) UHMWPE acetabular cup, respectively. At a visual inspection, one can observe the uniform BG61 coating of the entire acetabular cup (Fig. 3b), the surface of the UHMWPE cup being converted to a mat appearance.

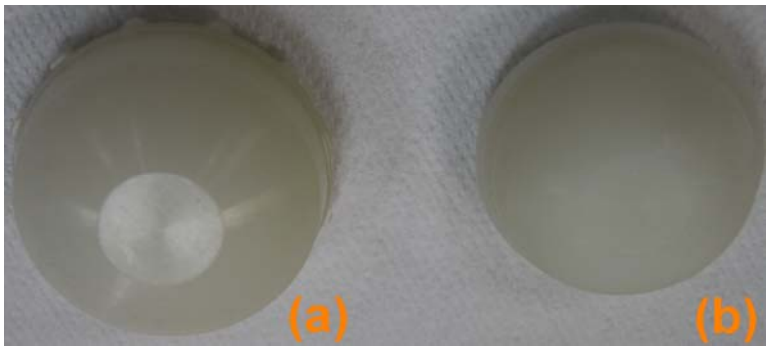

Fig. 3 – Photos of: a) bare; b) BG61 coated UHMWPE acetabular cup.

In Fig. 4, top-view SEM micrographs are presented at various magnifications for the bare UHMWPE acetabular cups (a, d, g), BG61 functionalized implants

(b, e, h), and BG61/UHMWPE structures immersed in SBF (c, f, i). The PLD functionalization of acetabular cups with BG61 coatings, transformed the rather uniform surface morphology of the implant, to a rough one consisting of round-shaped particulates with sizes in the range of (0.56–4.2) μm, which can provide a proper initial anchorage when growing cells *in situ*. The density was found to be of $(1.49 \pm 0.3) \times 10^{-7}$ particulates/cm^2.

After 42 days of immersion in SBF (Fig. 4c, f, i), the functionalized implant surface aspect was fully converted to an uniform envelope of very fine acicular grains. This is indicative of a bioactive behavior, being the result of a partial dissolution of the BG matrix, followed by the chemical growth in the biological fluid of a carbonated HA layer [13]. Thus, SEM observations confirmed the FTIR evidence (Fig. 2) which suggested the growth of a biomimetic HA layer on the implants' surface. In some cases, BG dissolution and CaP nucleation can be considered simultaneous processes [46]. The newly forming CaP deposits grow in time, and can fully or partially crystallize during a prolonged immersion in SBF.

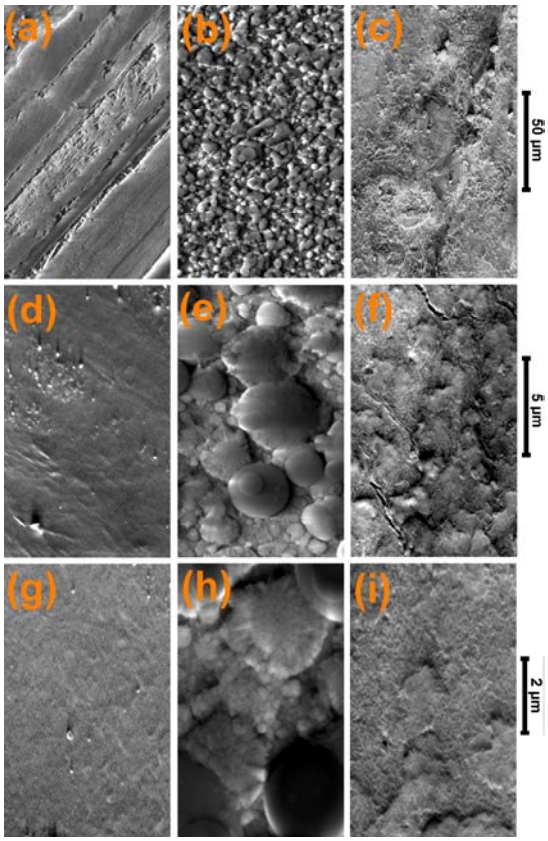

Fig. 4 – SEM micrographs of the UHMWPE acetabular cups: (a, d, g) bare; (b, e, h) biofunctionalized with BG61 films; (c, f, i) after 42 days of immersion in SBF.

3.2. EDS

EDS mapping of the films (data not presented here) revealed an uniform distribution of cationic species on film surface, indicating the absence of segregation phenomena, which are usually responsible for the formation of the undesirable secondary phases. The EDS spectra (Fig. 5a,b) demonstrated the purity of the deposited films. Indeed, apart from characteristic bone HA constituents (Ca, P, Na, Mg, K, O), no other elements (impurities) have been detected.

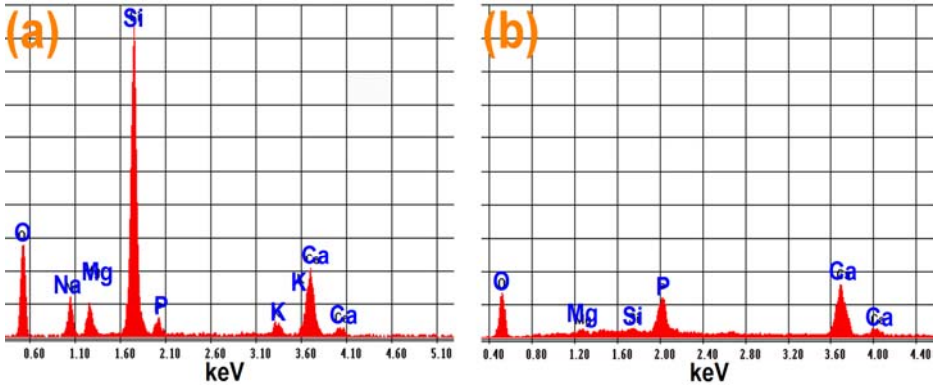

Fig. 5 – EDS spectra of BG61 coatings: a) as-deposited; b) after 42 days of immersion in SBF.

The quantitative EDS analyses (Table 3) revealed an excellent target-to-substrate atomic transfer. The targets composition was conserved in films, within the rather high error limits specific to EDS.

After immersion in SBF, dramatic compositional changes occurred (Fig. 5 and Table 3). They are: (*i*) a strong increase of Ca and P concentration (in good agreement with FTIR analysis which pointed to the HA chemical growth), (*ii*) the drastic diminution of Si content, and (*iii*) the absence of Na or K traces. On the other hand, the Mg content was not modified. The apparent conservation of the Mg concentration, after immersion in SBF, could suggest that this element does not play an active role in BG dissolution – HA precipitation process. However, one should not exclude the possibility of a partial substitution of Ca^{2+} ions by Mg^{2+} ions in the chemically grown HA layer. This hypothesis is supported by the lower value of the Ca/P atomic ratio after SBF immersion of ~1.47 as compared to the standard value of 1.67 characteristic to stoichiometric HA. The Ca substitution by Mg can also account for fine shift of IR bands in case of BG61 films immersed in SBF as compared to pure HA (visible in the inset to Fig. 2a). This could be related to the different radius of ≈ 114 pm for Ca^{2+} and of ≈ 86 pm for Mg^{2+} [47].

The Si presence for the BG61 functionalized cotyles tested in SBF is consistent with the bioactivity mechanism proposed by Hench [13]. It is involving the ion changes between the BG surface and surrounding physiological fluid (Na^{+},

Ca^{2+} cations of the glass for the H^+ and H_3O^+ from SBF), leading to the pH change in the vicinity of sample surface, and the partial dissolution of silicate network resulting in the formation of silanol (Si–OH) groups. The dissolution stage is followed by the Si–OH polycondensation resulting in a silica-rich layer, which catalyzes the nucleation and growth of the carbonated HA mix layer. The Si content (Table 3) seems therefore to originate from this bottom silica-rich layer, which served as the critical nucleation site for the apatitic layer growth.

Table 3

Comparison between the chemical composition (in at. %) and Ca/P atomic ratios of the BG61 target and coatings before and after the immersion in SBF

CONCENTRATION [at. %]	Si	Ca	P	Na	K	Mg	Ca/P ratio
BG61 target	53.62	11.85	4.46	17.52	3.13	9.42	~2.66
BG61 film (as-deposited)	57.7 ± 1.1	11.8 ± 1.0	3.9 ± 0.2	14.6 ± 1.0	2.3 ± 0.1	9.7 ± 0.3	~3.02
BG61 film (immersed in SBF)	6.0 ± 0.9	50.2 ± 2.1	34.2 ± 0.8	–	–	9.6 ± 2.0	~1.47

4. CONCLUSIONS

We have synthesized bioactive glass (BG) coatings onto commercial ultra high molecular weight polyethylene (UHMWPE) acetabular cup implants by Pulsed Laser Deposition using a SiO_2–Na_2O–K_2O–CaO–MgO–P_2O_5 BG compositional system, and tested them for 42 days by immersion in simulated body fluid, in homeostatic conditions. Structural (FTIR), morphological (SEM) and compositional (EDS) measurements assessed the PLD method feasibility for producing high quality implant coatings. The FTIR measurements showed highly depolymerized network for the BG which was able to induce the nucleation, growth and structuring of a biologically active apatite layer *in vitro*, with chemical composition resembling the one of human bone. The SEM investigations showed the conversion of the typical PLD film surface (consisting of round-shaped micrometric particulates) into a rough homogenous surface with an acicular aspect. The EDS analysis showed a remarkable nearly-stoichiometric transfer of the target composition to the BG deposited films.

Our findings demonstrate a high *in vitro* biomineralization capacity of the BG coating, favorable for a rapid osteointegration of implants. We conclude that BG/UHMWPE structures show promise for use as highly bioactive materials for applications in regenerative medicine.

Acknowledgements. The authors thank to Dr. Alain Aaron from FHi, France, for providing UHMWPE acetabular cups and to Dr. George Stan for performing the ATR-FTIR investigations as well as for the useful discussions. LD acknowledges the financial support from the Romanian

National Authority for Scientific Research, CNCS-UEFISCDI, Contract number TE 82/2011. LD and INM acknowledge with thanks the financial support of UEFISCDI Ideas Project no. 304/2011. LD acknowledges with thanks the financial support of UEFISCDI Ideas Project no. 337/2011. ACP acknowledges with thanks the financial support of PNII-RU-TE- 2011-3-0164 (TE 49/2011) research grant.

REFERENCES

1. J. A. Epinette, M. T. Manley, R. G. T. Geesink, *Fifteen years of clinical experience with hydroxyapatite coatings in joint arthroplasty*, Springer-Verlag, Paris, 2003.
2. B. León, J. Jansen, *Thin Calcium Phosphate Coatings for Medical Implants*, Springer, New York, 2010.
3. L. Duta, G. E. Stan, A. C. Popescu, G. Socol, F. M. Miroiu, I. N. Mihailescu, A. Ianculescu, I. Poeata, A. Chiriac, Proc. SPIE 888208, doi:10.1117/12.2032338 (2013).
4. C. Capuccini, P. Torricelli, F. Sima, E. Boanini, C. Ristoscu, B. Bracci, G. Socol, M. Fini, I.N. Mihailescu, A. Bigi, Acta Biomaterialia, **4**, 1885–1893 (2008).
5. L. E. Sima, G. E. Stan, C. O. Morosanu, A. Melinescu, A. Ianculescu, R. Melinte, J. Neamtu, S.M. Petrescu, J. Biomed. Mater. Res. A, **95**, 1203–1214 (2010).
6. L. Duta, G. Socol, F. Sima, I. N. Mihailescu, G. E. Stan, D. A. Marcov, L. E. Sima, S. M. Petrescu, A. Melinescu, A. Ianculescu, A. Chiriac, I. Poeata, IEEE Advanced Technologies for Enhancing Quality of Life (AT-EQUAL), 127–130, (2010); doi: 10.1109/ATEQUAL.2010.27.
7. J. Park, *Bioceramics: Properties, characterizations, and applications*, Springer, 2008.
8. H. L. Stein, *Ultra-high molecular weight polyethylene (UHMWPE), Guide to Engineering Plastics Families: Thermoplastic Resins*, Vol. 2: *Engineered Materials Handbook*, ASM International, 1999.
9. S. M. Kurtz, *The UHMWPE handbook: Ultra-high molecular weight polyethylene in total joint replacement*, Academic Press, 2004.
10. L. L. Hench, J. Wilson, *An introduction to bioceramics*, World Scientific Publishing Company, 1993.
11. J. R. Jones, A. Clare, *Bio-Glasses: An introduction*, John Wiley & Sons Ltd, 2012.
12. L. L. Hench, R. J. Splinter, W. C. Allen, T. K. Greenlee, J. Biomed. Mater. Res., **5**, 117–141 (1972).
13. L. L. Hench, J. Am. Ceram. Soc., **74**, 1487–1510 (1991).
14. L. L. Hench, Current Orthopaedics, **14**, 7–15 (2000).
15. M. Vallet-Regí, C. V. Ragel, A. J. Salinas, Eur. J. Inorg. Chem., **6**, 1029–1042 (2003).
16. L. L. Hench, *Fundamental aspects of biocompatibility*, CRC Press, 1981.
17. V. Cannillo, A. Sola, J. Eur. Ceram. Soc., **30**, 2031–2039 (2010).
18. L. Altomare, D. Bellucci, G. Bolelli, B. Bonferroni, V. Cannillo, L. De Nardo, R. Gadow, A. Killinger, L. Lusvarghi, A. Sola, N. Stiegler, J. Mater. Sci. - Mater. Med., **22**, 1303–1319 (2011).
19. J. R. J. Delben, K. Pereira, S. L. Oliveira, L. D. S. Alencar, A. C. Hernandes, A. A. S. T. Delben, J. Non-Cryst. Solids, **361**, 119–123 (2013).
20. A. Balamurugan, G. Balossier, J. Michel, J. M. F. Ferreira, Electrochim. Acta, **54**, 1192–1198 (2009).
21. F. Pishbin, A. Simchi, M. P. Ryan, A. R. Boccaccini, J. Eur. Ceram. Soc., **30**, 2963–2970 (2010).
22. G. E. Stan, A.C. Popa, D. Bojin, Dig. J. Nanomater. Bios., **5**, 557–566 (2010).
23. G. E. Stan, A. C. Popa, A. C. Galca, G. Aldica, J. M. F. Ferreira, Appl. Surf. Sci., **280**, 530–538 (2013).
24. A. C. Popescu, F. Sima, L. Duta, C. Popescu, I. N. Mihailescu, D. Capitanu, R. Mustata, L. E. Sima, S. M. Petrescu, D. Janackovic, Appl. Surf. Sci., **255**, 5486–5490 (2009).

25. J. Kwiatkowska, K. Suchanek, B. Rajchel, Acta Phys. Pol. A, **121**, 502–505 (2012).
26. J. V. Rau, R. Teghil, M. Fosca, A. De Bonis, I. Cacciotti, A. Bianco, V. R. Albertini, R. Caminiti, A. Ravaglioli, Mater. Res. Bull., **47**, 1130–1137 (2012).
27. A. C. Popescu, L. Duta, G. Dorcioman, I. N. Mihailescu, G. E. Stan, I. Pasuk, I. Zgura, T. Beica, I. Enculescu, A. Ianculescu, I. Dumitrescu, J. Appl. Phys., **110**, 064321 (2011).
28. A. Miotello, N. Patel, Appl. Surf. Sci., **278**, 19–25 (2013).
29. L. Floroian, F. Sima, M. Florescu, M. Badea, A. C. Popescu, N. Serban, I. N. Mihailescu, J. Electroanal. Chem., **648**, 111–118 (2010).
30. L. Duta, F. N. Oktar, G. E. Stan, G. Popescu-Pelin, N. Serban, C. Luculescu, I. N. Mihailescu, Appl. Surf. Sci., **265**, 41–49 (2012).
31. S. Lopez-Esteban, E. Saiz, S. Fujino, T. Oku, K. Suganuma, A. P. Tomsia, J. Eur. Ceram. Soc., **23**, 2921–2930 (2003).
32. D. Tanaskovic, B. Jokic, G. Socol, A. Popescu, I.N. Mihailescu, R. Petrovic, Dj. Janackovic, Appl. Surf. Sci., **254**, 1279–1282 (2007).
33. G. Socol, A. M. Macovei, F. Miroiu, N. Stefan, L. Duta, G. Dorcioman, I. N. Mihailescu, S. M. Petrescu, G. E. Stan, D. A. Marcov, A. Chiriac, I. Poeata, Mater. Sci. Eng. B, **169**, 159–168 (2010).
34. *** *Implants for surgery – In vitro evaluation for apatite-forming ability of implant materials*, ISO/FDIS 23317/2007.
35. T. Kokubo, H. Takadama, Biomaterials, **27**, 2907–2915 (2006).
36. M. Pino, N. Stingelin, K. E. Tanner, Acta Biomater., **4**, 1827–1836 (2008).
37. S. Agathopoulos, D. U. Tulyaganov, J. M. G. Ventura, S. Kannan, M. A. Karakassides, J. M. F. Ferreira, Biomaterials, **27**, 1832–1840 (2006).
38. G. Socrates, *Infrared and Raman characteristic group frequencies – Tables and Charts*, John Wiley & Sons Ltd, 2007.
39. G. E. Stan, I. Pasuk, M. A. Husanu, I. Enculescu, S. Pina, A. F. Lemos, D. U. Tulyaganov, K. El Mabrouk, J. M. F. Ferreira, J. Mater. Sci. – Mater. Med., **22**, 2693–2710 (2011).
40. J. Serra, P. González, S. Liste, S. Chiussi, B. León, M. Pérez-Amor, H. O. Ylänen, M. Hupa, J. Mater. Sci. - Mater. Med., **13**, 1221–1225 (2002).
41. M. Magallanes-Perdomo, A. H. De Aza, I. Sobrados, J. Sanz, P. Pena, Acta Biomater., **8**, 820–829 (2012).
42. M. Markovic, B. O. Fowler, M. S. Tung, J. Res. Natl. Inst. Stand. Technol., **109**, 553–568 (2004).
43. G. E. Stan, J. Optoelectron. Adv. M., **11**, 1132–1138 (2009).
44. E. Landi, G. Celotti, G. Logroscino, A. Tampieri, J. Eur. Ceram. Soc., **23**, 2931–2937 (2003).
45. M. Voltolini, H. -R. Wenk, J. Gomez Barreiro, S. C. Agarwal, J. Appl. Crystallogr., **44**, 928–934 (2011).
46. C. Berbecaru, H. V. Alexandru, G. E. Stan, D. A. Marcov, I. Pasuk, A. Ianculescu, Mat. Sci. Eng. B-Solid, **169**, 101–105 (2010).
47. *** http://en.wikipedia.org/wiki/Ionic_radius, last accessed: 2013-09-24.